The following publication Du, Y., Mak, C. M., & Li, Y. (2019). A multi-stage optimization of pedestrian level wind environment and thermal comfort with lift-up design in ideal urban canyons. Sustainable Cities and Society, 46, 101424 is available at https://doi.org/10.1016/j.scs.2019.101424.

A multi-stage optimization of pedestrian level wind environment and thermal comfort with lift-up design in ideal urban canyons

Abstract

Improvements for the pedestrian level wind environment and outdoor thermal comfort have become increasingly important in urban planning in light of concerns about global warming and urban heat island effects. Therefore, the goal of this study is to determine the optimum wind environment and outdoor thermal comfort for an ideal urban canyon in which the buildings have lift-up designs. A multi-stage optimization method is proposed consisting of three stages for the optimization process, e.g., surrogate model development, multi-objective optimization, and decision-making. An area weighted wind velocity parameter ($\overline{\mathrm{MVR}}$) and an outdoor thermal comfort parameter ($\overline{\mathrm{PET}}$) are chosen as the design objectives, and four design variables are selected. The response surface methodology combining computational fluid dynamics simulation results are used to fit surrogate models. The non-dominated sorting genetic algorithm is employed to find Pareto optimal solutions, and three decision-making strategies are adopted to determine the final optimum design solution in parallel. The optimization process of the ideal urban canyon confirms that the proposed method is highly effective to determine optimum building design in urban areas. The findings in this study are valuable for city-planners and policy-makers to build a sustainable urban living environment.

Keywords: *Lift-up design; Ideal urban canyon; Pedestrian level wind environment; Outdoor thermal comfort; Multi-stage optimization method*

Introduction

Rapid urban development has contributed to closely-spaced buildings in city districts, which inevitably modifies the outdoor microclimate at pedestrian level (Du and Mak, 2018a; Ng, 2009). The most significant impact is the obstruction of air movement within urban districts which affects the pedestrian level wind environment and outdoor thermal comfort subsequently (Blocken and Carmeliet, 2004; Niu et al., 2015). A good wind environment in city districts can improve wind comfort and help remove pollutants from urban canyons (Ai and Mak, 2015; Cui et al., 2017; Hang and Li, 2010). A good wind environment can also reduce the negative influence of urban heat island effect (Du et al., 2017a; Ignatius et al., 2015; O'Malley et al., 2015). This issue is most severe in high-density urban cities with climates that are hot and humid (Chatzidimitriou and Yannas, 2016; Elnabawi et al., 2016). Studies show that the average temperature in Hong Kong is rising, and the number of days with hot and humid weather has increased significantly compared to the past decades (Chan et al., 2012). Moreover, future projections forecast that extreme high temperature incidents will increase markedly in the future (Lee et al., 2011). Therefore, strategies to improve the pedestrian level wind environment and outdoor thermal comfort are of great significance.

To mitigate these problems, some strategies regarding to the layout of urban canyons have been applied in recent decades (Chatzidimitriou and Yannas, 2017; Mirzaei and Haghighat, 2010, 2011). Hang et al. (2009) investigated different urban morphologies via computational fluid dynamics (CFD) simulations, and determined that an oblique incident approaching wind results in a better wind environment in round-shaped cities than in other city shapes. Meanwhile, low building packing and low street aspect ratios were also found to be effective for enhancing the wind velocity in urban canyons (Du and Mak, 2018b; Ho et al., 2015; Kubota et al., 2008; Liu et al., 2005; Ramponi et al., 2015). Thus, the wind environment at pedestrian level can be improved by altering building configurations and urban layout.

The implementation of lift-up design into building configurations is a promising solution for improving pedestrian level wind environment and outdoor thermal comfort without sacrificing any valuable ground area (Du et al., 2017c). Lift-up designs, in which the building is elevated by pillars, have been extensively investigated (Du et al., 2017a; Du et al., 2018; Du et al., 2017c; Liu et al., 2017; Niu et al., 2015). Niu et al. (2015) conducted field measurements on a university campus, and observed that the lift-up design can markedly enhance the wind velocity at pedestrian level, while also providing enjoyable local spaces for outdoor activities during hot and humid summer. Du et al. (2017a) studied the influence of lift-up design on pedestrian level wind environment and outdoor thermal comfort on a complex university campus was studied by combining wind tunnel test results and on-site measurement results. The results clearly showed that the lift-up design could provide a pleasant microclimate in the hot and humid summer while not causing any cold stress in the winter. However, these studies applied only qualitative analysis methods. Subsequently, Du et al. (2018b) established a quantitative mathematical model for the relationship between lift-up design variables and wind comfort using a multi-variable optimization method. However, only the pedestrian level wind environment is considered during the optimization process. As the pedestrian level wind environment and outdoor thermal comfort are both important for urban planning, a multi-objective optimization for buildings with lift-up designs in the urban canyon should be conducted to deliver the final optimum building design.

Recently, response surface methodology (RSM) has been widely applied in computer experiments, particularly in the combination with CFD simulations (Simpson et al., 2001). Shen et al. (2012, 2013) optimized the ventilation rate of a livestock facility by coupling RSM approach with CFD simulations, and the statistical model developed using RSM approach was shown to represent the ventilation rate obtained from the CFD simulations very well. Sofotasiou et al. (2016) combined RSM with CFD simulations to determine the optimum window opening design to yield the best ventilation rate. The degree of influence of each design variables was identified, and the optimum ventilation rate was achieved. Therefore, combination of RSM with CFD simulation can be applied to find the optimal design for buildings.

To determine the geometric dimensions of an ideal urban canyon for the optimum wind environment and outdoor thermal comfort, a multi-stage optimization method is proposed in this study. The height of upper buildings, the spacing between buildings, the width of the lift-up cores, and the height of the lift-up cores are chosen as design variables. The dimensionless wind velocity parameter (area weighted mean wind velocity ratio,$\overline{\mathrm{MVR}}$) and outdoor thermal comfort parameter (area weighted Physiologically Equivalent Temperature, $\overline{\mathrm{PET}}$) are adopted as the two design objectives. The sampling process for the design points is based on the Design of Experiment (DOE) analysis. In particular, the Box-Behnken Design (BBD) is utilized for the RSM approach. Both a linear (first-order) model and a quadric (second-order) model are employed to fit the surrogate models. Moreover, the quality and goodness of the fitted surrogate models developed using RSM approach are evaluated through analysis of variance (ANOVA). The surrogate models are further coupled with the non-dominated sorting genetic algorithm (NSGA-II) to determine the

Pareto optimal design points. The final optimum design is determined using three decision-making strategies in parallel.

The reminder of this paper is organized as follows: after the introduction, the methodology and framework for the proposed multi-stage optimization method is presented in Section 2, along with the design variables and objective parameters. Section 3 establishes the verification of CFD simulation models used in this study. Section 4 presents results and discussion is shown in Section 5. Concluding remarks are given in in the final section.

2. Research design and methodology

2.1 Optimization framework

This study aims to develop a multi-stage optimization method to determine the optimum wind environment and thermal comfort around buildings with lift-up design in an ideal urban canyon. Fig. 1 shows the design framework for the multi-stage optimization method. There are three stages in this design framework: surrogate model development, multi-objective optimization, and decision-making.

In the first stage, the statistical models (RSM models) are established, as specified in a previous work (Du et al., 2018b). This includes establishment of the design of experiment (DOE), a reliable CFD simulation, and the RSM model. Specifically, for the establishment of the DOE: (a) the design variables, variable boundaries and design objectives should be determined first; and (b) an appropriate DOE scheme should be chosen, i.e., Central Composite Design (CCD), Box-Behnken Design (BBD), etc. Based on the generally good performance of BBD in the previous study (Du et al., 2018b), BBD is also utilized as the

DOE scheme in this study. After establishment of the DOE, a design dataset should be generated. Another important step in Stage 1 is the establishment of a reliable CFD simulation, which is a prerequisite for confident implementation of the optimization framework. This can be guaranteed by vigorously following the established best practice guidelines (BPGs) (Franke, 2007; Tominaga et al., 2008) and validating against a quality experimental dataset. After these steps, a first-order and second-order fitted regression model (surrogate model) can be developed from the dataset generated by the DOE and the corresponding values obtained from the CFD simulation by using the least square method and backward elimination method (EP, 1978). In particular, the analysis of variance (ANOVA) should be employed to exam the quality and goodness of fit of the RSM model.

In Stage 2, the NSGA-II (Deb et al., 2002) is utilized to conduct a multi-objective optimization of the statistical models established in Stage 1. NSGA-II is a multi-objective evolutionary algorithm based on the concept of Pareto dominance and optimality (Deb et al., 2002). The procedure for this algorithm can be summarised as follows: (i) create random new population, and evaluate and rank this population based on non-domination. (ii) Apply binary tournament selection, recombination, and mutation operators to generate the next offspring generation. (iii) From the first generation onwards, the new generations are created by combining the parent and offspring population to maintain elitism, identifying the non-dominated fronts, calculating crowding distance of the sorted solutions, and generating the next parent population. (iv) Repeat the above step until the maximum number of iteration is reached. A flowchart of the NSGA-II is presented in Fig.1, and detailed information regarding NSGA-II can be found in reference (Deb et al., 2002). In solving a multi-objective optimization problem, it is difficult to obtain the optimal values for all functions concurrently. Thus, special attention should be paid to the Pareto optimal solutions, which is a cluster of non-dominated solutions. Fig.2 shows the Pareto front for the concurrent minimization of two objectives. The solid red points are non-dominated solutions, and the open black points represent other possible solutions. More detailed information on the Pareto optimal front can be found in reference (Knowles and Corne, 1999).

In Stage 3, specific decision-making techniques (Shahhosseini et al., 2016), such as the Linear Programming Technique for Multidimensional Analysis of Preference (LINMAP), the Technique for Order of Preference by Similarity to Ideal Solution (TOPSIS), and the Shannon's Entropy techniques should be applied to determine the final optimum result from the Pareto optimal solutions obtained in Stage 2. In this study, the well-recognized LINMAP, TOPSIS, and Shannon's Entropy techniques are employed in parallel to obtain the final optimum result.

- LINMAP technique

For each Pareto optimal solution, the Euclidian distance to the ideal solution can be described as follows:

$$\mathrm{L}_{j+} = \sum_{j=1}^{k}(P_{ji} - P_i^{ideal})^2 \quad (1)$$

where, k stands for the total number of Pareto front solution; j is exact number of Pareto front solution, where $j = 1,2, \dots, k$; i is the number of objective, $i = 1, \dots, n$; P_{ji} is the value for ith objective and jth Pareto front solution; and P_i^{ideal} is the ideal value for ith objective. In the LINMAP decision-making technique, the result with the minimum Euclidian distance to the ideal solution is considered the final optimum result.

$$j_{final} = j \in \min(L_{j+}) \quad (2)$$

- TOPSIS technique

In contrast to Equation (1), the Euclidian distance to the non-ideal solution is used in this method:

$$\mathrm{L}_{j-} = \sum_{j=1}^{k} (P_{ji} - P_i^{non-ideal})^2 \quad (3)$$

The symbols in Equation (3) have the same meanings as in Equation (1).

An intermediate parameter is defined as follows:

$$\mathrm{EL}_j = \frac{L_{j-}}{L_{j-} + L_{j+}} \quad (4)$$

In the TOPSIS decision-making technique, the result with the maximum EL_j is designated as the final optimum result.

$$j_{final} = j \in \max(EL_j) \quad (5)$$

- Shannon’s entropy technique

Prior to the calculation of Shannon’s entropy, an intermediate parameter (q_{ji}) is defined as follows:

$$q_{ji} = \frac{P_{ji}}{\sum_{j=1}^{k} P_{ji}} \; j = 1,2,\dots,k, \; i = 1,\dots,n \quad (6)$$

The definition for the symbols in Equation (6) are the same as Equation (1).

Shannon’s entropy (EN_i) for ith objective is defined as follows:

$$EN_i = -\frac{1}{\ln(k)} \sum_{j=1}^{k} q_{ji} \ln(q_{ji}) \quad (7)$$

The deviation degree (DE_i) for ith objective can be written as follows:

$$DE_i = 1 - EN_i \tag{8}$$

The weight coefficient for ith objective can be given as follows:

$$WE_i = \frac{DE_i}{\sum_{i=1}^{n} DE_i} \tag{9}$$

Thus, the new assessment factor (F_{ji}) is used instead of P_{ji} during further process, which is defined as follows:

$$F_{ji} = P_{ji} \times WE_i \tag{10}$$

Then, the TOPSIS is used to obtain the final optimum result from the Pareto frontier solution by rank the new weighted assessment factor (F_{ji}).

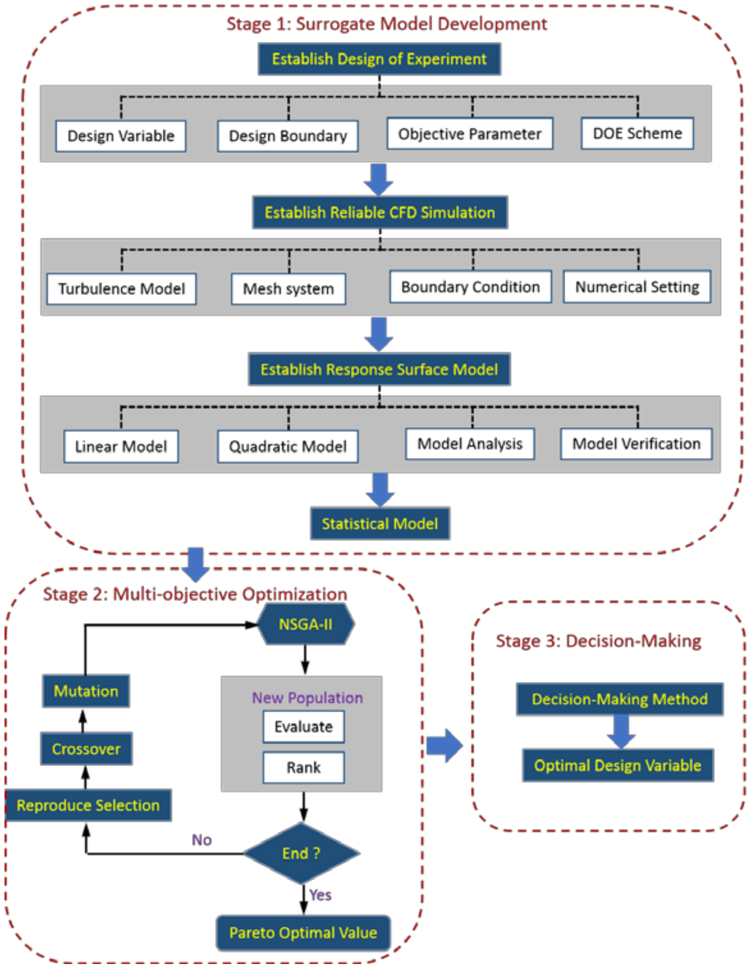

Fig. 1 Proposed multi-stage optimization design framework.

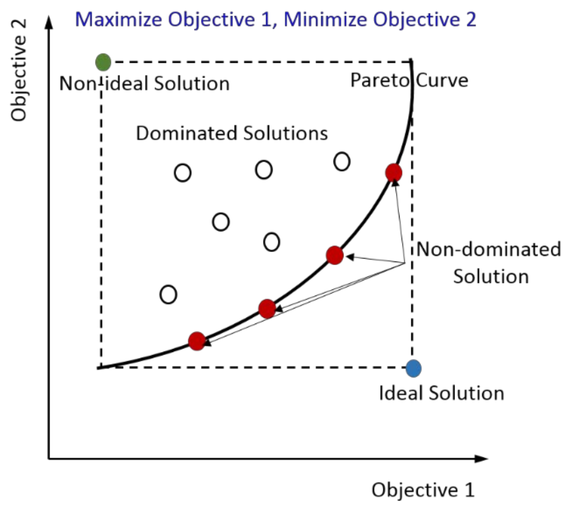

Fig. 2 Pareto front for two objectives.

2.2 Response surface methodology (RSM)

A fully-developed d-order RSM approach for four design variables based on a Taylor series approximation can be expressed as follows (Gunst, 1996):

$$f(X) = \hat{\alpha}_0 + \sum_{i=1}^{n} \hat{\alpha}_i x_i + \sum_{i=1}^{n} \hat{\alpha}_{ii} {x_i}^2 + \sum_{i=1}^{n} \sum_{j>i} \hat{\alpha}_{ij} x_j x_i + \sum_{i=1}^{n} \sum_{j>i} \sum_{k>j} \hat{\alpha}_{ijk} x_k x_j x_i + \sum_{i=1}^{n} \sum_{j>i} \sum_{k>j} \sum_{l>k} \hat{\alpha}_{ijkl} x_l x_k x_j x_i + \cdots + \sum_{i=1}^{n} \hat{\alpha}_{i,\dots,i} x_i^d \quad (11)$$

where, $X = (x_i, x_j, x_k, x_l)$, in which x_i, x_j, x_k, x_l are the design variables; $f(X)$ is the estimated response value; and $\hat{\alpha}$ is an estimated coefficient of the RSM model. In this study, Equation (11) is used to fit the RSM model.

The above RSM model can also be expressed as the following form:

$$\hat{f} = K\hat{\alpha} \quad (12)$$

here, $\hat{f}$ is a n × 1 vector; K is a n × m matrix; and $\hat{\alpha}$ is an m × 1 vector.

The estimated coefficient $\hat{\alpha}$ based on the least square method can be written as follows:

$$\hat{\alpha} = (K'K)^{-1}K'f \quad (13)$$

The variance of estimated response value ($\hat{f}(X)$) can be given by Equation (14) as follows:

$$Var\ \hat{f}(X) = \sigma^2 x_i'(K'K)^{-1}x_i \quad (14)$$

where, $\hat{f}(X)$ is the corresponding response value of x_i; and σ^2 is the estimated error.

2.3 Description of the urban canyon

In this study, an ideal urban canyon with lift-up design underneath buildings is developed based on a study conducted by the University of Hamburg (CEDVAL B1-1), which examined airflows within regular arrays of obstacles in the BLASIUS wind tunnel

(Leitl, 1998). The physical model of the ideal urban canyon is illustrated in Fig. 3, in which the buildings are constructed at a scale ratio of 1:200. A total of 21 uniform buildings with lift-up design are aligned in an arrangement with three buildings in the crosswind direction and seven buildings along the wind direction, evenly spaced (equal face-to-face gaps, D) in both the stream-wise and span-wise directions. A schematic description of each building is shown in Fig. 3 (b) and Fig. 3 (c). The lift-up design used in this study has three cores, in keeping with previous studies (Du et al., 2018b).

The design variables in this study are the height of the upper building (H_B), the street spacing between buildings (face-to-face gaps, D), the height of the lift-up core (H_C), and the width of the lift-up core (W_C). For the upper part of each building, the width (W_B) is kept constant, while the height (H_B) is changed during the optimization process. For the lift-up core, both the geometric dimensions of width (W_C) and height (H_C) vary. The design variables, are listed in Table 1 along with the design constants. Note that the values in Table 1 are for the full scale. The key factor that determines the airflow pattern around the buildings is the aspect ratio, which is defined as the ratio of the building height to the street spacing. It can be seen that the ratio of the building height/street spacing ($\mathrm{H/D}$, where $\mathrm{H} = H_B + H_c$) is in the range of 0.1 to 3. This covers the three flow regions (Oke, 1988): the isolated roughness flow region, the wake interference flow region and the skimming flow region. Moreover, the ranges of lift-up core heights and widths are adopted from a previous study (Du et al., 2018b). The lower bound of the lift-up height is selected based on the actual lift-up height (4 m in prototype) (Du et al., 2017a), and the upper bound of height is chosen as the height of two stories (8 m in prototype) since the land use efficiency is very vital to the scarce urban resources (Ng, 2009).

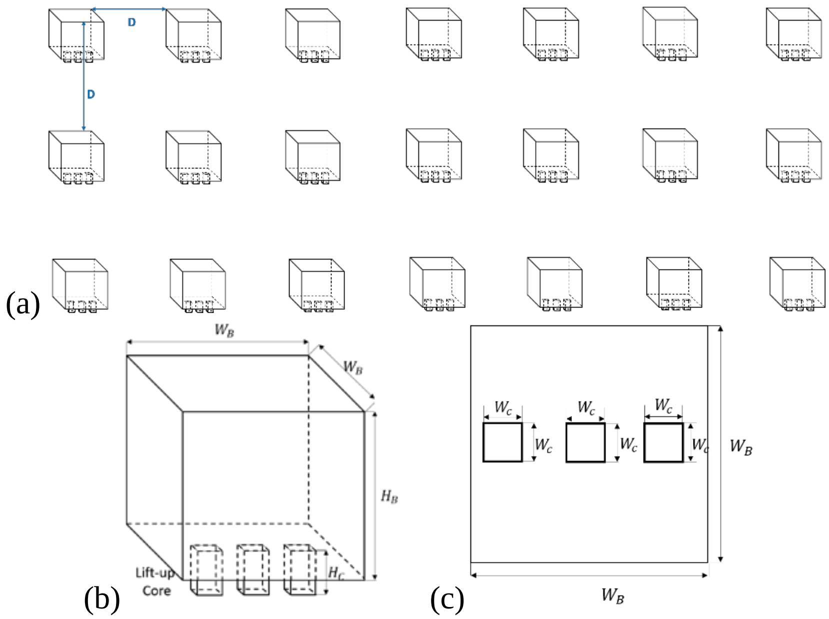

Fig. 3 (a) Schematic diagram of the ideal urban canyon; (b) 3-D view of an isolated building with lift-up design; (c) plan view of an isolated building with lift-up design.

Table 1. Summary of building design parameters

Design Variables	Lower Limit	Upper Limit	Description
D(m)	50	150	Face-to-face gaps between buildings
H_B(m)	15	150	Height of upper building
H_C(m)	4	8	Height of lift-up core
W_C(m)	1	4	Width of lift-up core
Design Constant	Value		
W_B(m)	20		Width of upper building

2.4 Description of objective parameters

To evaluate the wind environment at pedestrian level (2 m in this study), the mean wind velocity ratio (MVR) is utilized in this study. It is a dimensionless velocity magnitude, which is defined as the pedestrian level wind velocity normalized to a reference wind velocity (Du et al., 2017b). This dimensionless parameter can be expressed as follows:

$$MVR = V_p/V_r \tag{15}$$

where, V_p stands for the velocity magnitude at pedestrian level; and V_r is the velocity magnitude at a reference height (200 m in this study).

The bio-meteorological index, PET, is used in this study to represent the thermal comfort owning to its direct translation of thermal stress (Höppe, 1999; Matzarakis et al., 1999). The calculation of PET is based on the energy balance of human body, and the free software RayMan (Matzarakis et al., 2007, 2010) is used to calculate the PET values in this study. Environmental parameters including air temperature (T_a, ℃), relative humidity (RH, %), mean radiant temperature (T_{mrt}, ℃), and wind velocity (V_a, m/s) are required as input parameters for calculating PET values. In addition, thermal-physiological parameters are also required, including physiological information (sex, age, height, etc.), clothing insulation level (I_{clo}, ℃), and activity type (metabolic rate, W). The wind velocity predicted in the CFD simulation is used as the input wind velocity for calculating PET (Liu et al., 2016), and the values of MVR should be converted to in-situ values. The average wind velocity is 5 m/s at 200 reference height in Hong Kong (Du et al., 2017c). Based on the work of Willemsen and Wisse (2007), the following relationship can be established for a quality CFD simulation:

$$MVR_{CFD} = MVR_{in-situ} \tag{16}$$

Because the hot and humid summer is more concerned by the city residents than the temperate winter in subtropical cities, especially in sunny summer days (Cheng et al., 2012). Thus, only hot and sunny summer conditions are considered in this study, and mean values of the parameters measured on a sunny summer day (22 August, 2016) in Hong Kong from our previous study (Du et al., 2017a) are used here. These parameters were measured at two sites: the ground area and the lift-up area underneath the upper building. The mean measured results for the environmental parameters and the thermal-physiological parameters used in this study are summarized in Table 2. The environmental parameters measured at the ground area are used for the building surrounding areas, while the environmental parameters measured in the lift-up area are utilized for the area underneath the elevated upper buildings in this study (Du et al., 2017a; Liu et al., 2016). More detailed information regarding the on-site measurements can be found in reference (Du et al., 2017a).

Table 2 Summary of the parameters used for calculating PET values

Environmental Parameters	Ground	Lift-up
Air temperature (T_a, ℃)	32.8	31.1
Relative humidity (RH, %)	86.7	83
Mean radiant temperature (T_{mrt}, ℃)	58.1	31.6
Thermal-physiological Parameters		
Age	35	
Height (m)	1.75	
Weight (kg)	75	
Metabolic rate (W)	69.8	
Clothing level (clo)	0.3	

The area within the ideal urban canyons is the target region, as shown in Fig. 4. To quantitatively represent the pedestrian level wind environment and outdoor thermal comfort, the area-weighted MVR ($\overline{MVR}$) and PET ($\overline{\mathrm{PET}}$) are utilized as the objective parameters. The definitions of $\overline{MVR}$ and $\overline{\mathrm{PET}}$ can be described as follows:

$$\overline{MVR} = \int \widetilde{MVR}\, dA/A \tag{17}$$

$$\overline{\mathrm{PET}} = \int \widetilde{PET}\, dA/A \tag{18}$$

where, $\widetilde{MVR}$ and $\widetilde{PET}$ are the values of MVR and PET, respectively, at any location at pedestrian level; and A is the area of the target region. The annual wind velocity at 200m (reference height) is 5 m/s (Du et al., 2017c), and wind becomes annoyance when the wind velocity is higher than 5 m/s (Willemsen and Wisse, 2007). Thus, the value of $\overline{MVR}$ should be smaller than 1. However, higher wind velocity is much appreciated in Hong Kong as explained in the introduction part. It is therefore the goal of this optimization is to obtain high $\overline{MVR}$ (less than 1) and low $\overline{\mathrm{PET}}$ values.

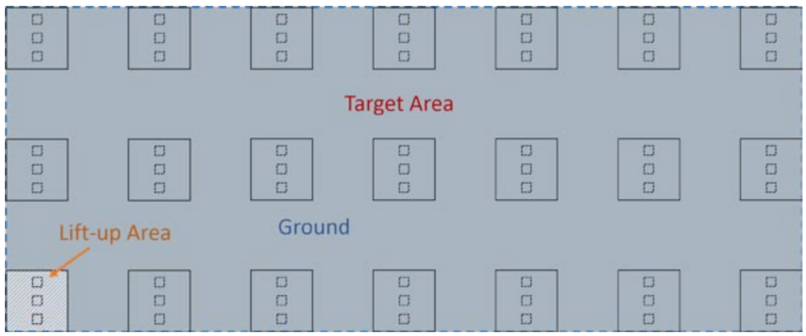

Fig. 4. Schematic show of the target region.

3. CFD validation

3.1 Turbulence model

In this study, the widely-used steady Reynolds-averaged Navier-Stokes (RANS) turbulence model is used to predict the airflows around buildings. This model was chosen for its generally good performance in simulating airflows and its economic computational cost (Blocken et al., 2016; Du et al., 2017c; Tominaga and Stathopoulos, 2009). Specifically, the two-equation RANS model, i.e., the re-normalization group (RNG) $k - \varepsilon$turbulence model, is used owning to its adaptiveness in solving rapid strain and streamline curvatures (Fluent, 2010). This adaptiveness is realized by inclusion of an additional strain-dependent term (R_ε), which can be described as follows:

$$R_\varepsilon = \frac{C_\mu \rho \eta^3 (1-\eta/\eta_0)\varepsilon^2}{(1+\beta\eta^3)k} \tag{19}$$

where, model constants C_μ, η_0, and β are 0.085, 4.38, and 0.012, respectively; ρ is the fluid density; and $\eta \equiv Sk/\varepsilon$ where S is the strain rate scale.

3.2 Description of the validation model

Experimental data from wind tunnel test of CEDVAL B1-1 conducted by the University of Hamburg is used here for validation (Leitl, 1998). The airflow of a neutrally stratified atmospheric boundary layer over an array of 3D buildings was simulated during these wind tunnel tests. A total of 21 buildings were arranged in a configuration with three buildings aligned in the crosswind direction and seven buildings aligned along the wind direction. The geometries and dimensions of the buildings and their layout are shown in Fig. 5. The buildings are uniform with dimensions of $\mathrm{H} \times \mathrm{W} \times \mathrm{L} = 0.125 \times 0.15 \times 0.1$ m (in model scale), where H, W, and L are the height, width, and length, respectively. The building spacing was 0.1 m in model scale. All buildings were constructed at a scale ratio of 1:200, which is also used for the CFD simulations in this study. The measurements conducted on the horizontal plane (Z=0.0625 m in model scale) were used for validation purpose in this study. The six validation lines are specifically illustrated in Fig. 5.

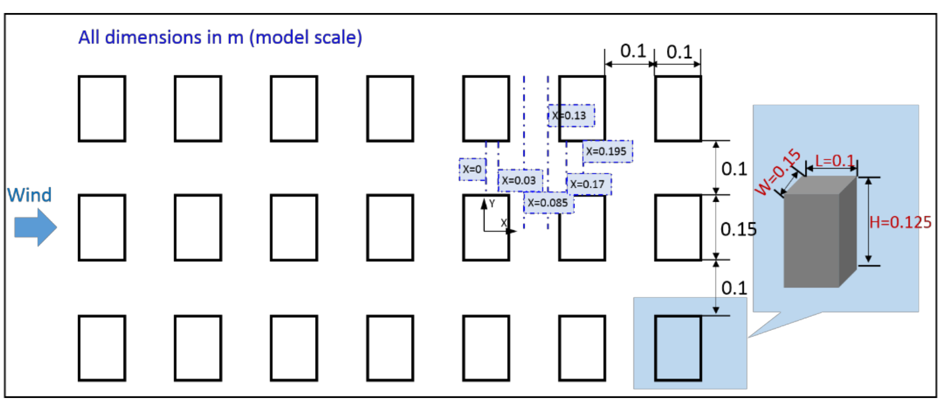

Fig. 5 Building layout during wind tunnel tests: top view.

3.3 Boundary conditions and numerical details

The inflow boundary profiles of the wind velocity (U), turbulent kinetic energy (k), and turbulent dissipation rate (ε) can be specified by fitting Equations (20-22) to the experimental data given in reference (Leitl, 1998). Thus, z_0=0.0007 m, u^*=0.37772 m/s, $C_1 = 0.025$, and $C_2 = 0.41$.

$$U = u^*/\kappa \times \{ln\,(z + z_0)/z_0\} \tag{20}$$

$$k = \sqrt{C_1 \cdot \ln(z + z_0) + C_2} \tag{21}$$

$$\varepsilon = \{u^*\sqrt{C_\mu}/\kappa(z + z_0)\} \cdot \sqrt{C_1 \cdot \ln(z + z_0) + C_2} \tag{22}$$

where z_0 is the aerodynamic roughness height (m); u^* is the friction velocity (m/s); κ is the von Karman constant, which is equal to 0.4187; C_μ is a constant equal to 0.09; and C_1 and C_2 are constants which are equal to 0.025 and 0.41, respectively.

The computational domain is constructed to numerically simulate the airflow around the buildings, and is shown in Fig. 6 along with its boundary conditions. This computational domain conforms to the requirements of BPGs for a steady RANS simulation. Structural hexahedral cells were utilized to discretize the computational domain. The pressure and momentum equations were coupled using the SIMPLEC algorithm, and second-order upwind schemes were utilized for the convective and diffusion terms. The calculations were considered converged when all residuals were below 10^{-5} and the monitored points in the computational domain were stable for more than 100 iterations.

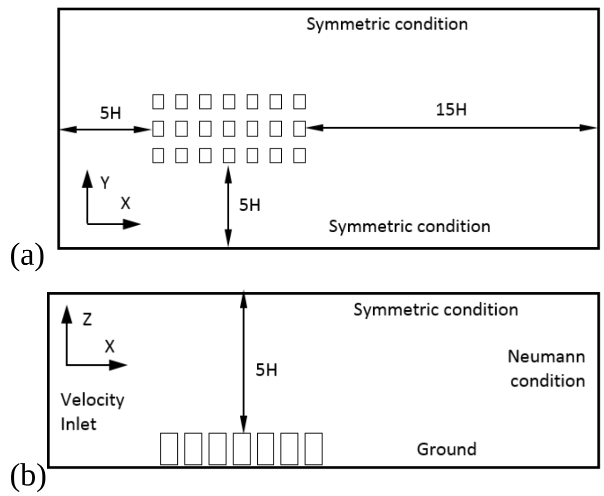

Fig. 6 Schematic view of the computational domain: (a) top view; and (b) side view.

3.4 Mesh sensitivity test

A systematic mesh sensitivity test was carried out with minimum grid sizes of 0.0003 m, 0.0005 m, and 0.001 m, corresponding to total cell numbers of 3.2 million, 5.6 million, and 8.2 million cells, respectively. The details of the three mesh systems are shown in Fig. 7, and prediction results for the three mesh systems are shown in Fig. 8. In Fig. 8, the horizontal axis is presented in dimensionless form, and U_{ref} is the wind velocity at reference height. The results show that the difference between 0.0005 m and 0.0003 m mesh system is subtle, while the differences between the 0.001 m mesh system and other two mesh systems are obvious. Thus, a minimum grid size of 0.0005 m is sufficiently fine for the CFD simulation.

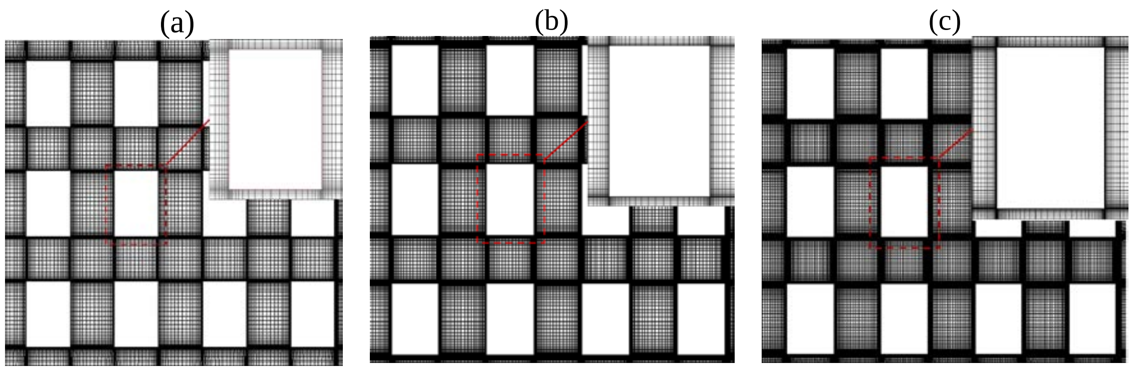

Fig. 7 Mesh details for the three mesh systems: (a) minimum grid size of 0.001 m; (b) minimum grid size of 0.0005 m; (c) minimum grid size of 0.0003 m.

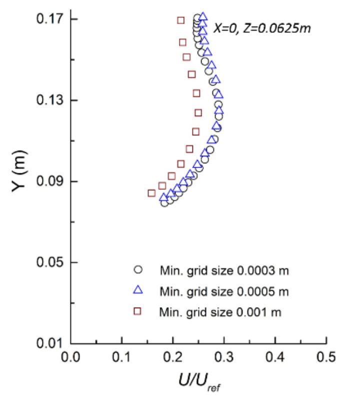

Fig. 8 Mesh sensitivity test results.

3.5 Validation results

Fig.9 presents a comparison of the results for the dimensionless velocity on the horizontal plane at $\mathrm{Z} = 0.0625$ m (model scale). It can be seen that the predicted results from CFD simulation are in good agreement with the wind tunnel test data, except for few points. Most of the discrepancies between the CFD results and the experimental results are within 10%, which can be considered as reliable and confident CFD simulation results (Franke, 2007; Tominaga et al., 2008). Therefore, the CFD simulation is capable of accurately predicting the airflow around buildings for this type of urban canyon.

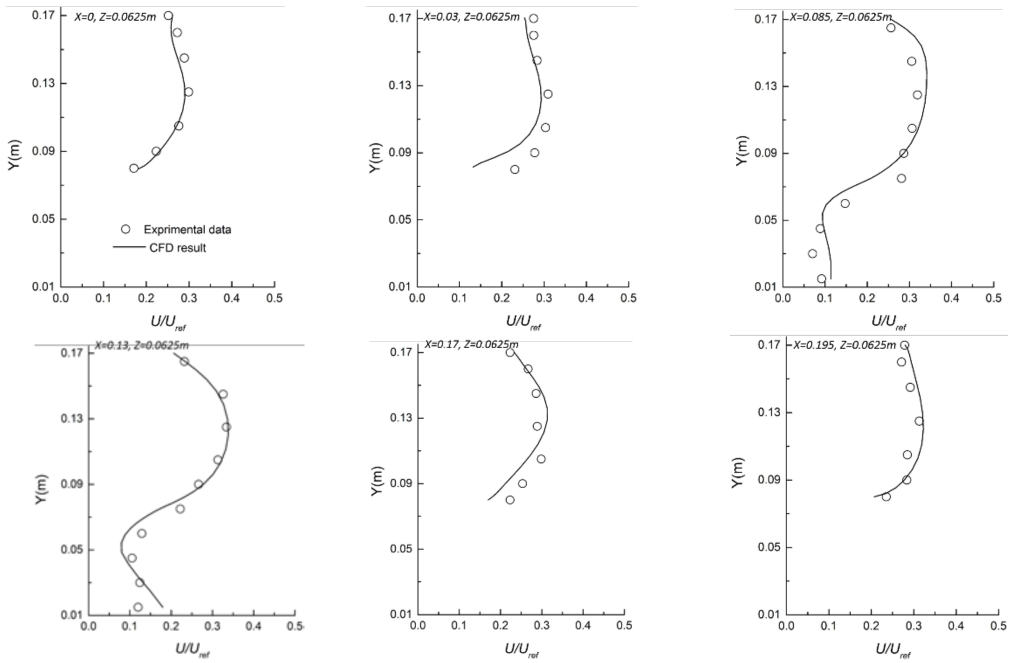

Fig. 9 Comparison results of dimensionless velocity on horizontal plane.

4. Results

This section presents the results obtained from the developed multi-stage optimization method. The computational settings and the inflow wind profiles are the same as validation case in order to ensure the CFD simulation reliability.

4.1 Surrogate model development

As a commonly used computational experimental designs, the Box-Behnken design (BBD) performs well for establishing the relationship between response results and relevant variables. Some studies have also verified that the BBD design is reliable for model development demanding moderate design points (Du et al., 2018b; Shen et al., 2012, 2013). To develop a confident RSM model with economical computational cost, BBD design is adopted in this study and Design Experts software is utilized. Table 3 summarizes the dataset created by the BBD design along with the corresponding results obtained from the CFD simulation. Note that the centre design point was repeated several times in this process.

Table 3. BBD-based design dataset and corresponding CFD results

Design Points (full scale)				CFD Results	
H_B(m)	D (m)	H_C(m)	W_C(m)	$\overline{\mathrm{MVR}}$	$\overline{\mathrm{PET}}$(℃)
150	150	6	2.5	0.30	46.2
82.5	50	6	1	0.31	42.1
82.5	50	6	4	0.19	43.3
82.5	150	4	2.5	0.41	47.2
82.5	50	4	2.5	0.20	42.5
15	100	6	4	0.39	45.1
82.5	50	8	2.5	0.26	42.8
150	100	8	2.5	0.25	43.9
82.5	150	6	1	0.49	46.0
82.5	100	4	1	0.37	44.5
82.5	100	8	4	0.25	45.2
15	100	6	1	0.49	44.1
150	100	4	2.5	0.22	44.0
150	100	6	4	0.17	44.9
82.5	100	6	2.5	0.37	44.7
82.5	150	6	4	0.40	46.8
82.5	100	4	4	0.31	45.1
150	100	6	1	0.32	44.5
15	100	8	2.5	0.41	44.6
82.5	150	8	2.5	0.43	46.8
82.5	100	8	1	0.44	43.5
15	100	4	2.5	0.40	44.5
150	50	6	2.5	0.20	42.3
15	50	6	2.5	0.30	43.0
15	150	6	2.5	0.51	45.8

After performing the CFD simulation for the required design points in Table 3, the data in Table 3 is utilized to develop the surrogate model for $\overline{\mathrm{MVR}}$ and $\overline{\mathrm{PET}}$. A linear (first-order) model and quadratic (second-order) model are used to fit the data, and backward regression is employed to remove insignificant terms. Table 4 and Table 5 present developed surrogate models for $\overline{\mathrm{MVR}}$ and $\overline{\mathrm{PET}}$, respectively. In addition, the goodness of the surrogate models to the predicted CFD values are evaluated by the Predicted R^2 and Adjusted R^2, which are parameters adopted from regression analysis (Lovric, 2011). The closer the R^2 values are to 1, the better the predictive ability of the surrogate model will be. As indicated in Table 4 and Table 5, the surrogate models formulated with the linear model have low values of R^2, which means that the linear surrogate models are unsuitable. However, the surrogate models formulated with the quadratic model are in good agreement with the results of the CFD simulation. Thus, the surrogate models developed with the quadratic model are used in this study.

Table 4 Developed surrogate models for $\overline{\mathrm{MVR}}$

Surrogate model	Model vs. simulation results
Linear (first-order) model	
$\overline{MVR} = 0.338 - 5.7\times10^{-4}H_B + 1.05\times10^{-3}D + 4.58\times10^{-3}H_c - 0.037W_c$	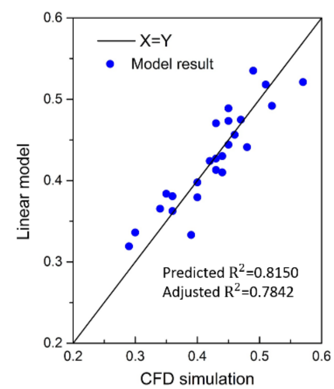
Quadratic (second-order) model	
$\overline{MVR} = -5.9\times10^{-3} + 9.98\times10^{-6}H_B + 3.05\times10^{-3}D + 0.074H_c - 0.014W_c - 7.4\times10^{-6}H_BD - 1.7\times10^{-4}H_BW_c + 2.67\times10^{-4}DW_c - 5.83\times10^{-3}H_cW_c - 8\times10^{-7}H_B^2 - 6.5\times10^{-6}D^2 - 4.56\times10^{-3}H_c^2$	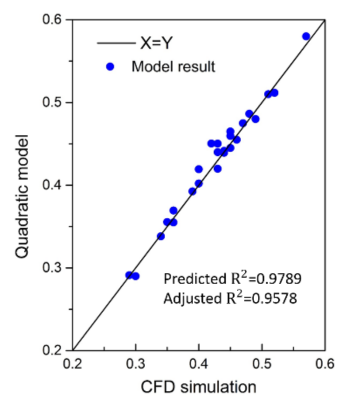

Table 5. Developed surrogate models for $\overline{\mathrm{PET}}$

Surrogate model	Model vs. simulation results
Linear (first-order) model $\overline{PET} = 40.24 - 1.23 \times 10^{-3} H_B + 0.051 D - 0.108 H_c + 0.2 W_c$	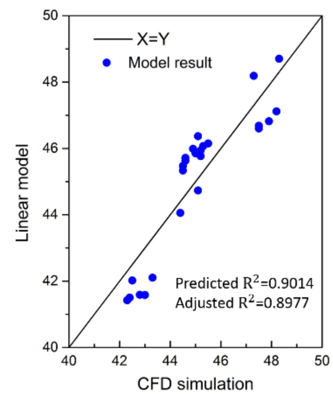
Quadratic (second-order) model $\overline{PET} = 40.99 - 5.43 \times 10^{-3} H_B + 0.037 D + 0.128 H_c - 0.346 W_c + 8.15 \times 10^{-5} H_B D - 3 \times 10^{-3} D H_c + 0.067 H_c W_c - 4 \times 10^{-5} H_B^2 + 5 \times 10^{-5} D^2 - 8.54 \times 10^{-3} H_c^2 + 0.0719 W_c^2$	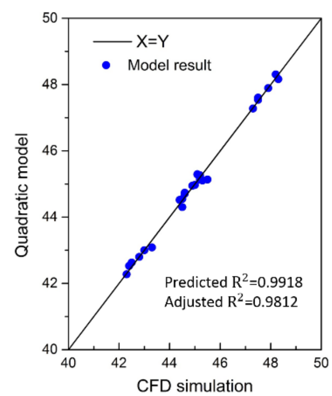

The adequacy of the developed surrogate models can be evaluated using the analysis of variance (ANOVA), which is checked at a 95% level of confidence. Table 6 presents the ANOVA results for the developed surrogate models. It can be seen that the p-values for regressions are less than 0.0001 (with F-ratio values of greater than 50), which suggests that the developed surrogate models are significant and good to fit. In addition, the p-values for the lack-of-fit tests are greater than 0.2 (>0.05), further indicating that the developed surrogate models are adequate.

Table 6. Analysis of variance (ANOVA) for the developed surrogate models

	Variation source	F-ratio	P-value	Significance
Surrogate model for $\overline{\mathrm{MVR}}$	Regression	60.84	<0.0001	Significant
	Lack-of-fit	1.93	0.2712	Not significant
Surrogate model for $\overline{\mathrm{PET}}$	Regression	53.14	<0.0001	Significant
	Lack-of-fit	2.32	0.2295	Not significant

4.2 Verification of surrogate models

To verify the reliability of the developed surrogate models, seven datasets within the design space are chosen randomly, as listed in Table 7. The values of deviation between the values predicted by the surrogate model and CFD method are also listed in Table 7. As Table 7 indicates, the values predicted by the surrogate models and the results obtained from the CFD simulations are in good agreement, which confirms the reliability of the developed surrogate models for $\overline{\mathrm{MVR}}$ and $\overline{\mathrm{PET}}$.

Table 7. Verification datasets for the developed surrogate models

Design Points (full scale)				$\overline{\mathrm{MVR}}$			$\overline{\mathrm{PET}}$		
H_B(m)	D (m)	H_C(m)	W_C(m)	CFD	Model	Deviation	CFD	Model	Deviation
120	120	7	3	0.30	0.31	3.3%	45.0	45.1	0.2%
70	80	5	3	0.31	0.31	0.0%	43.7	44.0	0.7%
110	130	5	2	0.39	0.37	5.1%	45.9	45.5	0.9%
60	110	8	4	0.35	0.33	5.7%	45.7	45.5	0.4%
50	70	6	2	0.33	0.35	6.1%	43.6	43.3	0.7%
80	70	4	1	0.31	0.32	3.2%	43.2	43.1	0.2%
20	140	7	2	0.55	0.53	3.6%	45.6	45.3	0.7%

4.3 Correlation of design parameters

The Parameters Correlation analysis (Agresti, 2003) is used here to obtain the effect of each design variable on design objectives, e.g. $\overline{MVR}$ and $\overline{\mathrm{PET}}$. The Latin Hypercube Sampling method is utilized to generate 100 unique and random data sets with 5% deviation of correlation (Agresti, 2003). This data set is then used by the Spearman's rank correlation method to determine the influence extent of the design variables on the corresponding design objectives. The obtained correlation values for the design parameters are listed in Table 8. The negative values in Table 8 means that the design objective will decrease when the design variable increase. It can be seen that the absolute values of design variable D is the biggest both for $\overline{MVR}$ and $\overline{\mathrm{PET}}$ among the four design variables. This means that the face-to-face gaps between buildings has the most influence for pedestrian level wind environment and outdoor thermal comfort. Besides, the height of upper building is the second most influential factor for evaluating $\overline{MVR}$ while the width of lift-up core becomes the second most influential factor for evaluating $\overline{\mathrm{PET}}$. Further, the height of lift-up core is the least influential factor for evaluating $\overline{MVR}$ while the height of upper building is the least influential factor for evaluating $\overline{\mathrm{PET}}$. In addition, the correlations between each design variables are evaluated. The absolutes value between these variables are around zero, which confirms the independence of the design variables.

Table 8 Correlation values between the design parameters

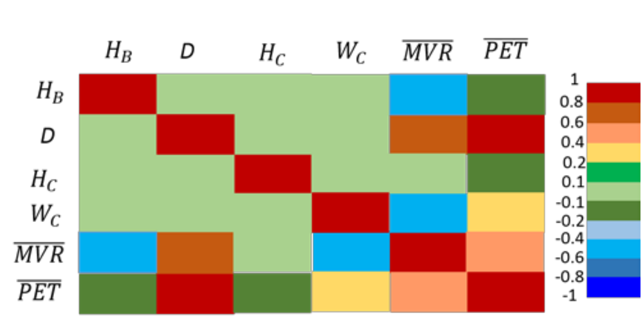

Design objective	Design variable	Correlation value
$\overline{MVR}$	H_B	-0.58
	D	0.64
	H_C	0.07
	W_C	-0.41
$\overline{\mathrm{PET}}$	H_B	-0.14
	D	0.90
	H_C	-0.19
	W_C	0.26

4.4 Multi-objective optimization

To reach the goal of double-objective optimization, the value of $\overline{\mathrm{MVR}}$ should be minimized and the value of $\overline{\mathrm{PET}}$ should be optimized. This is achieved using a multi-objective genetic algorithm (NSGA-II). The parameters adopted for the NSGA-II algorithm are summarised in Table 9.

Table 9. Parameters used in the NSGA-II algorithm

Parameter	Value
Population size	200
Maximum generation	500
Tournament size	10
Crossover probability	0.9
Mutation probability	0.1
Pareto fraction	0.6

The Pareto front for the double-objective optimization of $\overline{\mathrm{MVR}}$ and $\overline{\mathrm{PET}}$ is shown in Fig. 10. The trade-off between the $\overline{\mathrm{MVR}}$ and $\overline{\mathrm{PET}}$ values can be identified from the Pareto optimal front. The variation ranges of $\overline{\mathrm{MVR}}$ and $\overline{\mathrm{PET}}$ values in the Pareto optimal solution are 0.32 to 0.56 and 41.4 to 44.9, respectively.

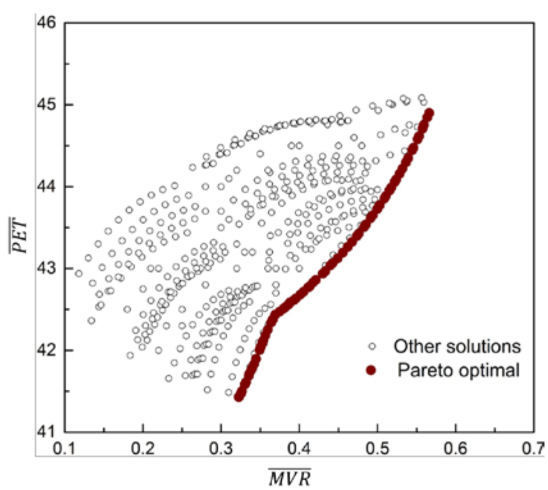

Fig.10 Pareto optimal front for $\overline{\mathrm{MVR}}$ and $\overline{\mathrm{PET}}$.

4.5 Optimum result

Prior to any decision-making for the final optimum solution, dimensions of the two objectives should be unified. Thus, the Euclidian technique (Li et al., 2015) is utilized for normalising the dimensions and scales here. The Pareto frontier values obtained in Section

4.3 are denoted as P_{ji}, where j is the index for each Pareto frontier value and i is the index for each objective ($i = 1{,}2$). Thus, the dimensionless objective $P_{ji}{}'$ can be defined as follows:

$$P_{ji}{}' = P_{ji} \Big/ \sqrt{\sum_{j=1}^{k} P_{ji}^2} \tag{23}$$

here, the definition for each symbol is the same as Equation (1).

After the normalisation, the LINMAP, TOPSIS and Shannon's entropy decision-making techniques are used to obtain the final optimum solution. The optimal values within the design space are then calculated based on the three decision-making techniques, as indicated in Fig.11 along with the ideal and non-ideal solution points.

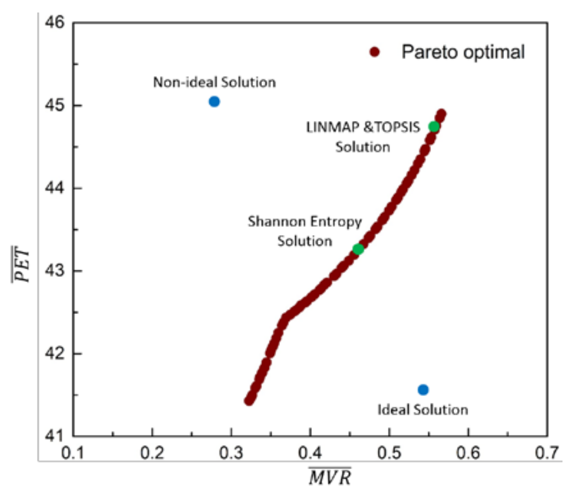

Fig. 11 Application of three decision-making techniques for Pareto optimal front.

In order to select the final optimum solution, the deviation from the results obtained from three decision-making techniques to the ideal solution is used here:

$$s = \frac{\sqrt{\sum_{i=1}^{2}(P_i - P_i^{Ideal})^2}}{\sqrt{\sum_{i=1}^{2}(P_i - P_i^{Ideal})^2} + \sqrt{\sum_{i=1}^{2}(P_i - P_i^{Non-ideal})^2}} \tag{24}$$

where, P_i is optimal solution obtained from three decision-making techniques; P_j^{Ideal} and $P_j^{Non-ideal}$ are the ideal and non-ideal solutions indicated in Fig.11.

The deviation values for the LINMAP, TOPSIS and Shannon's entropy decision-making techniques are 0.957, 0.957 and 0.517, respectively. Thus, the results obtained from the Shannon's entropy decision-making technique is the final optimum solution. Accordingly, the optimum design set is H_B is 70 m, D is 108 m, H_c is 8 m and W_c is 1 m, which yields the optimum $\overline{MVR}$ and $\overline{\text{PET}}$ values is 0.45 and 43.4. It can be seen that the optimum height of lift-up core and the width of the lift-up core has reached its upper and lower boundary, which further confirms the results obtained from our previous study (Du et al., 2018b).

5. Discussion

Throughout the application of the optimization method, only summer sunny day is considered since this is the most concerned for subtropical city under the background of global warming and urban heat island effect. Because the multi-stage optimization method is closely coupled with outdoor wind environment and thermal comfort, its further application is restricted by local wind climate and weather condition. Basically, this method can also be applied to different climate and the influence of different weather condition on optimal building designs should be taken into consideration.

The ideal urban canyon is used as a case study to illustrate the proposed multi-stage optimization method. The buildings are given as uniform in this paper, and only the aerodynamic characteristics between the buildings and wind flow are considered. However, this multi-stage optimization method can also be applied to other conditions with different design variables and different design objectives. For instance, the shapes and numbers of lift-up core should be considered in our future works. Moreover, the other objectives can also be included in the optimization method, like building life-cycle payback or structural feasibility. In addition, this case study only focuses on improving pedestrian level low wind environment and hot outdoor thermal comfort. However, pedestrian safety should also be considered in urban planning, such as the strong gust event. Further studies are still needed for considering pedestrian safety as a design objective.

6. Conclusion

This study aims to determine the building configuration for the optimum pedestrian level wind environment and outdoor thermal comfort in an ideal urban canyon in which each building has a lift-up design. A multi-stage optimization framework is proposed, consisting of three stages for the optimization process, e.g., surrogate model development, multi-objective optimization, and decision-making. Four design variables are varied simultaneously during the optimization process: the height of the upper building, the spacing between buildings, the height of the lift-up cores, and the width of the lift-up cores. The pedestrian level wind environment and outdoor thermal comfort are used as the design objectives. For the CFD simulations, the steady RANS turbulence model is used owning to its modelling accuracy and economical computational costs. The NSGA-II algorithm is employed to obtain the Pareto optimal design sets.

The main findings of this study can be summarized as follows: (i) the surrogate models are established by combining the RSM approach and CFD simulation results, and their adequacy are evaluated by ANOVA. The quadric model developed by combining the RSM approach and CFD simulation results performs better than the linear model for both surrogate models. (ii) The surrogate models developed in Stage 1 are in good agreement with CFD simulation results. (ii) Three decision-making techniques are utilized to determine the final optimum design point: LINMAP, TOPSIS, and Shannon's entropy techniques. Among the three decision-making techniques, the design solution obtained by the Shannon's entropy decision-making technique yields the minimum deviation from the ideal solution. (iii) Among these design variables, the face-to-face gaps between buildings has (D) the most influence for pedestrian level wind environment and outdoor thermal comfort. (iv) Within the design space, the final optimum design solution for the ideal urban canyon is that the height of upper building is 70 m, the buildings spacing is 108 m, the height of lift-up core is 8m, and the width of lift-up core is 1 m. Accordingly, the final optimum value for $\overline{\text{MVR}}$ and $\overline{\text{PET}}$ is 0.45 and 43.4.

In general, these results clearly demonstrate that the proposed multi-stage optimization method can be successfully used to determine an optimum design solution for multiple objectives in an ideal urban canyon. Moreover, this study can serve as a good demonstration of the application of this optimization method, which can certainly be applied for other similar studies. In addition, the proposed multi-stage optimization method can assist urban planners and policy-makers in promoting urban environmental sustainability.

Acknowledgements

The work described in this paper was fully supported by a grant from the Research Grants Council of the Hong Kong Special Administrative Region, China (Project No. C5002-14G).

Reference

Agresti, A., 2003. Categorical data analysis. John Wiley & Sons.

Ai, Z., Mak, C.M., 2015. From street canyon microclimate to indoor environmental quality in naturally ventilated urban buildings: issues and possibilities for improvement. *Building and environment* 94, 489-503.

Blocken, B., Carmeliet, J., 2004. Pedestrian wind environment around buildings: Literature review and practical examples. *Journal of Thermal Envelope and Building Science* 28, 107-159.

Blocken, B., Stathopoulos, T., Van Beeck, J., 2016. Pedestrian-level wind conditions around buildings: Review of wind-tunnel and CFD techniques and their accuracy for wind comfort assessment. *Building and Environment* 100, 50-81.

Chan, H., Kok, M., Lee, T., 2012. Temperature trends in Hong Kong from a seasonal perspective. *Climate Research* 55, 53-63.

Chatzidimitriou, A., Yannas, S., 2016. Microclimate design for open spaces: Ranking urban design effects on pedestrian thermal comfort in summer. *Sustainable Cities and Society* 26, 27-47.

Chatzidimitriou, A., Yannas, S., 2017. Street canyon design and improvement potential for urban open spaces; the influence of canyon aspect ratio and orientation on microclimate and outdoor comfort. *Sustainable cities and society* 33, 85-101.

Cheng, V., Ng, E., Chan, C., Givoni, B., 2012. Outdoor thermal comfort study in a sub-tropical climate: a longitudinal study based in Hong Kong. *International journal of biometeorology* 56, 43-56.

Cui, D., Mak, C.M., Ai, Z., Kwok, K.C., Meng, X., Niu, J., 2017. On-site evaluation of pedestrian-level air quality at a U-type street canyon in an ancient city. *Journal of Wind Engineering and Industrial Aerodynamics* 168, 322-333.

Deb, K., Pratap, A., Agarwal, S., Meyarivan, T., 2002. A fast and elitist multiobjective genetic algorithm: NSGA-II. *IEEE transactions on evolutionary computation* 6, 182-197.

Du, Y., Mak, C.M., 2018a. Improving pedestrian level low wind velocity environment in high-density cities: A general framework and case study. *Sustainable Cities and Society*.

Du, Y., Mak, C.M., Huang, T., Niu, J., 2017a. Towards an integrated method to assess effects of lift-up design on outdoor thermal comfort in Hong Kong. *Building and Environment* 125, 261-272.

Du, Y., Mak, C.M., Kwok, K., Tse, K.-T., Lee, T.-c., Ai, Z., Liu, J., Niu, J., 2017b. New criteria for assessing low wind environment at pedestrian level in Hong Kong. *Building and Environment* 123, 23-36.

Du, Y., Mak, C.M., Li, Y., 2018b. Application of a multi-variable optimization method to determine lift-up design for optimum wind comfort. *Building and Environment* 131, 242-254.

Du, Y., Mak, C.M., Liu, J., Xia, Q., Niu, J., Kwok, K.C., 2017c. Effects of lift-up design on pedestrian level wind comfort in different building configurations under three wind directions. *Building and Environment* 117, 84-99.

Elnabawi, M.H., Hamza, N., Dudek, S., 2016. Thermal perception of outdoor urban spaces in the hot arid region of Cairo, Egypt. *Sustainable cities and society* 22, 136-145.

EP, B.G., 1978. Statistics for experimenters: an introduction to design, data analysis, and model building.

Fluent, A., 2010. ANSYS FLUENT 13.0 Theory Guide, Turbulence., in: ANSYS Inc, C., PA (Ed.).

Franke, J., 2007. Best practice guideline for the CFD simulation of flows in the urban environment. Meteorological Inst.

Gunst, R.F., 1996. Response surface methodology: process and product optimization using designed experiments. Taylor & Francis.

Hang, J., Li, Y., 2010. Ventilation strategy and air change rates in idealized high-rise compact urban areas. *Building and Environment* 45, 2754-2767.

Hang, J., Sandberg, M., Li, Y., 2009. Effect of urban morphology on wind condition in idealized city models. *Atmospheric Environment* 43, 869-878.

Ho, Y.-K., Liu, C.-H., Wong, M.S., 2015. Preliminary study of the parameterisation of street-level ventilation in idealised two-dimensional simulations. *Building and Environment* 89, 345-355.

Höppe, P., 1999. The physiological equivalent temperature–a universal index for the biometeorological assessment of the thermal environment. *International journal of Biometeorology* 43, 71-75.

Ignatius, M., Wong, N.H., Jusuf, S.K., 2015. Urban microclimate analysis with consideration of local ambient temperature, external heat gain, urban ventilation, and outdoor thermal comfort in the tropics. *Sustainable Cities and Society* 19, 121-135.

Knowles, J., Corne, D., 1999. The pareto archived evolution strategy: A new baseline algorithm for pareto multiobjective optimisation, Evolutionary Computation, 1999. CEC 99. Proceedings of the 1999 Congress on. IEEE, pp. 98-105.

Kubota, T., Miura, M., Tominaga, Y., Mochida, A., 2008. Wind tunnel tests on the relationship between building density and pedestrian-level wind velocity: Development of guidelines for realizing acceptable wind environment in residential neighborhoods. *Building and Environment* 43, 1699-1708.

Lee, T.-c., Chan, K.-y., Ginn, W.-l., 2011. Projection of extreme temperatures in Hong Kong in the 21st century. Acta Meteorologica Sinica 25, 1-20.

Leitl, B., Schatzmann, M., 1998. CEDVAL at Hamburg University. http://www.mi.unihamburg.de/Data-Sets.432.0.html. Accessed June 12 2018.

Li, Y., Liao, S., Liu, G., 2015. Thermo-economic multi-objective optimization for a solar-dish Brayton system using NSGA-II and decision making. *International Journal of Electrical Power & Energy Systems* 64, 167-175.

Liu, C.-H., Leung, D.Y., Barth, M.C., 2005. On the prediction of air and pollutant exchange rates in street canyons of different aspect ratios using large-eddy simulation. *Atmospheric Environment* 39, 1567-1574.

Liu, J., Niu, J., Mak, C.M., Xia, Q., 2017. Detached eddy simulation of pedestrian-level wind and gust around an elevated building. *Building and Environment* 125, 168-179.

Liu, J., Niu, J., Xia, Q., 2016. Combining measured thermal parameters and simulated wind velocity to predict outdoor thermal comfort. *Building and Environment* 105, 185-197.

Lovric, M., 2011. International Encyclopedia of Statistical Science. Springer.

Matzarakis, A., Mayer, H., Iziomon, M.G., 1999. Applications of a universal thermal index: physiological equivalent temperature. *International journal of biometeorology* 43, 76-84.

Matzarakis, A., Rutz, F., Mayer, H., 2007. Modelling radiation fluxes in simple and complex environments—application of the RayMan model. *International journal of biometeorology* 51, 323-334.

Matzarakis, A., Rutz, F., Mayer, H., 2010. Modelling radiation fluxes in simple and complex environments: basics of the RayMan model. *International journal of biometeorology* 54, 131-139.
Mirzaei, P.A., Haghighat, F., 2010. A novel approach to enhance outdoor air quality: pedestrian ventilation system. *Building and Environment* 45, 1582-1593.
Mirzaei, P.A., Haghighat, F., 2011. Pollution removal effectiveness of the pedestrian ventilation system. *Journal of Wind Engineering and Industrial Aerodynamics* 99, 46-58.
Ng, E., 2009. Policies and technical guidelines for urban planning of high-density cities–air ventilation assessment (AVA) of Hong Kong. *Building and environment* 44, 1478-1488.
Niu, J., Liu, J., Lee, T.-c., Lin, Z.J., Mak, C.M., Tse, K.-T., Tang, B.-s., Kwok, K.C., 2015. A new method to assess spatial variations of outdoor thermal comfort: Onsite monitoring results and implications for precinct planning. *Building and Environment* 91, 263-270.
O'Malley, C., Piroozfar, P., Farr, E.R., Pomponi, F., 2015. Urban Heat Island (UHI) mitigating strategies: A case-based comparative analysis. *Sustainable Cities and Society* 19, 222-235.
Oke, T.R., 1988. Street design and urban canopy layer climate. *Energy and buildings* 11, 103-113.
Ramponi, R., Blocken, B., Laura, B., Janssen, W.D., 2015. CFD simulation of outdoor ventilation of generic urban configurations with different urban densities and equal and unequal street widths. *Building and Environment* 92, 152-166.
Shahhosseini, H.R., Farsi, M., Eini, S., 2016. Multi-objective optimization of industrial membrane SMR to produce syngas for Fischer-Tropsch production using NSGA-II and decision makings. *Journal of Natural Gas Science and Engineering* 32, 222-238.
Shen, X., Zhang, G., Bjerg, B., 2012. Investigation of response surface methodology for modelling ventilation rate of a naturally ventilated building. *Building and Environment* 54, 174-185.
Shen, X., Zhang, G., Bjerg, B., 2013. Assessments of experimental designs in response surface modelling process: estimating ventilation rate in naturally ventilated livestock buildings. *Energy and Buildings* 62, 570-580.
Simpson, T.W., Poplinski, J., Koch, P.N., Allen, J.K., 2001. Metamodels for computer-based engineering design: survey and recommendations. *Engineering with computers* 17, 129-150.
Sofotasiou, P., Calautit, J.K., Hughes, B.R., O'Connor, D., 2016. Towards an integrated computational method to determine internal spaces for optimum environmental conditions. *Computers & Fluids* 127, 146-160.
Tominaga, Y., Mochida, A., Yoshie, R., Kataoka, H., Nozu, T., Yoshikawa, M., Shirasawa, T., 2008. AIJ guidelines for practical applications of CFD to pedestrian wind environment around buildings. *Journal of wind engineering and industrial aerodynamics* 96, 1749-1761.
Tominaga, Y., Stathopoulos, T., 2009. Numerical simulation of dispersion around an isolated cubic building: Comparison of various types of k–ε models. *Atmospheric Environment* 43, 3200-3210.
Willemsen, E., Wisse, J.A., 2007. Design for wind comfort in The Netherlands: Procedures, criteria and open research issues. *Journal of Wind Engineering and Industrial Aerodynamics* 95, 1541-1550.